MATHEMATICAL METHODS IN THE APPLIED SCIENCES
Math. Meth. Appl. Sci. 2008; **31**:2095–2114
Published online 25 March 2008 in Wiley InterScience
(www.interscience.wiley.com) DOI: 10.1002/mma.1008
MOS subject classification: 49 Q 10; 49 K 20; 49 M 15; 65 K 10

Analytical and numerical methods in shape optimization‡

Helmut Harbrecht*, †

Institut für Numerische Simulation, Universität Bonn, Wegelerstr. 6, 53115 Bonn, Germany

SUMMARY

This paper is intended to overview on analytical and numerical methods in shape optimization. We compute and analyse the shape Hessian in order to distinguish well-posed and ill-posed shape optimization problems. We introduce different discretization techniques of the shape and present existence and convergence results of approximate solutions in case of well posedness. Finally, we survey on the efficient numerical solution of the state equation, including finite and boundary element methods as well as fictitious domain methods.

KEY WORDS: shape optimization; optimality conditions; shape calculus

Dedicated to Wolfgang L. Wendland on the occasion of his 70th birthday

1. INTRODUCTION

Shape optimization is quite important for aircraft design, bridge construction, electromagnetic shaping, etc. Many problems that arise in applications, particularly in structural mechanics, can be formulated as the minimization of functionals defined over a class of admissible domains. Such problems have been intensively studied in the literature in the past 25–30 years (see [1–4], and the references therein). Especially, the development of efficient algorithms in shape optimization is of growing interest.

This survey article is dedicated to analytical and numerical methods in shape optimization. We will view the shape optimization problem as an optimization problem in a Banach space by identifying the shape with its parameterization with respect to a fixed reference domain. By using a second-order shape calculus we are able to compute the shape Hessian. Our ansatz ensures that the shape Hessian denotes in fact the second-order Fréchet derivative of the given shape

*Correspondence to: Helmut Harbrecht, Institut für Numerische Simulation, Universität Bonn, Wegelerstr. 6, 53115 Bonn, Germany.
†E-mail: harbrecht@ins.uni-bonn.de
‡This paper was originally intended to be a part of the special issue on Analysis and Numerics of Boundary Integral Equations, dedicated to Wolfgang L. Wendland on the occasion of his 70th birthday.

 Received 25 November 2007

functional. Depending on the properties of the shape Hessian we can distinguish well-posed and ill-posed shape optimization problems. In case of well posedness we are able to prove existence of approximate shapes and their convergence to the optimal domain.

We illustrate well posedness and ill posedness by two examples. Stationary free boundary problems, especially Bernoulli's free boundary problem (see, e.g. [5, 6]) or electromagnetic shaping (see e.g. [7–9]), are generally well-posed problems. Whereas we will show that compactly supported shape problems, such as L^2- or gradient-tracking functionals, are ill posed.

We present several numerical methods to solve the underlying state equation in an efficient way. Depending on the problem under consideration we propose to solve the state equation by boundary element methods (BEMs), by the coupling of BEMs and finite element methods (FEMs), or by fictitious domain methods (FDMs). We emphasize that all these methods have in common that they are *meshless*, that is, they do not need an explicit triangulation of the varying domain. Consequently, large domain deformations are realizable without remeshing. For the sake of completeness, we also discuss the use of FEMs.

This paper is organized as follows. Section 2 is dedicated to shape calculus. By computing first- and second-order shape derivatives, we are able to analyze the shape optimization problem at hand. Depending on the coercivity estimates of the shape Hessian we will distinguish between well-posed and ill-posed problems. Both cases are illustrated by a corresponding example. Section 3 is concerned with the discretization techniques of the shape. In particular, in case of well posedness, we show that approximate shapes converge quasi-optimal with respect to the energy norm induced by the shape Hessian. Finally, Section 4 addresses the efficient numerical solution of the state equation.

In the following, in order to avoid the repeated use of generic but unspecified constants, by $C \lesssim D$ we mean that C can be bounded by a multiple of D, independently of parameters which C and D may depend on. Obviously, $C \gtrsim D$ is defined as $D \lesssim C$, and $C \sim D$ as $C \lesssim D$ and $C \gtrsim D$.

2. ANALYZING SHAPE OPTIMIZATION PROBLEMS

2.1. Shape calculus

Let $\Omega \subset \mathbb{R}^n$, $n = 2, 3$, denote a sufficiently smooth simply connected domain with boundary $\Gamma := \partial\Omega$. Throughout this paper we shall focus on the following shape functional:

$$J(\Omega) = \int_\Omega j(\mathbf{x}, u(\mathbf{x}))\, \mathrm{d}\mathbf{x} \to \min \tag{1}$$

where the state function u satisfies the boundary value problem

$$-\Delta u = f \ \text{ in } \Omega, \quad u = g \ \text{ on } \Gamma \tag{2}$$

Herein, we assume that $f, g : \mathbb{D} \to \mathbb{R}$ and $j : \mathbb{D} \times \mathbb{R} \to \mathbb{R}$ are sufficiently smooth functions, where $\mathbb{D} \subset \mathbb{R}^n$ denotes the hold all.

Remark 1

The hold all $\mathbb{D}$ is assumed to be a closed subset of $\mathbb{R}^n$ and serves first as the domain of definition for all data in order to make the underlying shape problem well defined. It is assumed to be sufficiently large such that all domains of an iterative solution process for (1) are contained.

DOI: 10.1002/mma

For a sufficiently smooth domain perturbation field $\mathbf{V}:\Omega\to\mathbb{R}^n$ we can define the perturbed domain $\Omega_\varepsilon[\mathbf{V}]$ as

$$\Omega_\varepsilon[\mathbf{V}]:=\{(\mathbf{I}+\varepsilon\mathbf{V})(\mathbf{x}):\mathbf{x}\in\Omega\},\quad \varepsilon>0$$

Then, the shape derivative of functional (1) in the direction $\mathbf{V}$ is defined as the limes

$$\nabla J(\Omega)[\mathbf{V}]=\lim_{\varepsilon\to 0}\frac{J(\Omega_\varepsilon[\mathbf{V}])-J(\Omega)}{\varepsilon}$$

For $f\in C(\overline{\Omega})$ the directional shape derivative of the domain integral $\int_\Omega f(\mathbf{x})\,\mathrm{d}\mathbf{x}$ is the boundary integral

$$\nabla\left(\int_\Omega f(\mathbf{x})\,\mathrm{d}\mathbf{x}\right)[\mathbf{V}]=\int_\Gamma\langle\mathbf{V},\mathbf{n}\rangle f(\mathbf{x})\,\mathrm{d}\sigma_{\mathbf{x}}$$

Here, $\mathbf{n}$ denotes the outward unit normal to the boundary Γ and $\langle\cdot,\cdot\rangle$ is the Euclidean inner product in $\mathbb{R}^n$. Thus, by the product rule we obtain

$$\nabla J(\Omega)[\mathbf{V}]=\int_\Gamma\langle\mathbf{V},\mathbf{n}\rangle j(\mathbf{x},g)\,\mathrm{d}\sigma_{\mathbf{x}}+\int_\Omega\frac{\partial j}{\partial u}(\mathbf{x},u)\,\mathrm{d}u[\mathbf{V}]\,\mathrm{d}\mathbf{x}\tag{3}$$

Here, $\mathrm{d}u[\mathbf{V}]$ is the *local shape derivative*, defined pointwise by

$$\mathrm{d}u(\mathbf{x})[\mathbf{V}]=\lim_{\varepsilon\to 0}\frac{u_\varepsilon[\mathbf{V}](\mathbf{x})-u(\mathbf{x})}{\varepsilon},\quad \mathbf{x}\in\Omega\cap\Omega_\varepsilon$$

It reads as

$$\Delta\,\mathrm{d}u[\mathbf{V}]=0\ \text{ in }\Omega,\quad \mathrm{d}u[\mathbf{V}]=\langle\mathbf{V},\mathbf{n}\rangle\frac{\partial(g-u)}{\partial\mathbf{n}}\ \text{ on }\Gamma\tag{4}$$

cf. [10–12]. We introduce the adjoint state function p according to

$$-\Delta p=\frac{\partial j}{\partial u}(\cdot,u)\ \text{ in }\Omega,\quad p=0\ \text{ on }\Gamma\tag{5}$$

and apply Green's second formula to the second term of the right-hand side in (3). Thus, in view of (4) and (5), we derive the boundary integral representation of the shape derivative

$$\nabla J(\Omega)[\mathbf{V}]=\int_\Gamma\langle\mathbf{V},\mathbf{n}\rangle\left\{j(\mathbf{x},g)+\frac{\partial p}{\partial\mathbf{n}}\frac{\partial(g-u)}{\partial\mathbf{n}}\right\}\mathrm{d}\sigma_{\mathbf{x}}\tag{6}$$

We observe that the directional derivative lives completely on the free boundary, involving the Dirichlet-to-Neumann maps (often called the Steklov–Poincaré operator) of u and p. Consequently, as observed first by Hadamard [13], the shape gradient is a functional defined on the free boundary. In particular, it is obvious that it suffices to consider only boundary variations $\mathbf{V}:\Gamma\to\mathbb{R}^n$.

2.2. Second-order derivatives

In order to discuss sufficient optimality conditions one has to take the shape Hessian into account. To this end, we introduce an $(n-1)$-dimensional reference manifold $\widehat{\Gamma}\subset\mathbb{R}^n$ and consider a fixed

DOI: 10.1002/mma

boundary perturbation field, for example, in the direction of the outward normal $\widehat{\mathbf{n}}$. We suppose that the free boundary can be parameterized via a sufficiently smooth function r in terms of

$$\boldsymbol{\gamma}:\widehat{\Gamma}\to\Gamma,\quad \boldsymbol{\gamma}(\mathbf{x})=\mathbf{x}+r(\mathbf{x})\widehat{\mathbf{n}}(\mathbf{x}) \tag{7}$$

That is, we can identify a domain with the scalar function r. Defining the standard variation

$$\boldsymbol{\gamma}_\varepsilon:\widehat{\Gamma}\to\Gamma_\varepsilon,\quad \boldsymbol{\gamma}_\varepsilon(\mathbf{x}):=\boldsymbol{\gamma}(\mathbf{x})+\varepsilon\,\mathrm{d}r(\mathbf{x})\widehat{\mathbf{n}}(\mathbf{x}) \tag{8}$$

where $\mathrm{d}r$ is again a sufficiently smooth scalar function, we obtain the perturbed domain $\Omega_\varepsilon[\mathrm{d}r]$. Consequently, both the shapes and their increments, can be seen as elements of a Banach space X. It turns out that we require $X=C^{2,\alpha}(\widehat{\Gamma})$ for some $\alpha>0$ in the present case of pde-constraint shape functionals such as (1), (2).

A quite canonical choice is to take the unit sphere

$$\mathbb{S}:=\{\widehat{\mathbf{x}}\in\mathbb{R}^n:\|\widehat{\mathbf{x}}\|=1\}$$

as reference manifold, which corresponds to the restriction to star-shaped domains. This choice will be considered in the sequel. Here and in the sequel, $\widehat{\mathbf{x}}$ will always indicate a point on the unit sphere. In particular, for a point $\mathbf{x}\in\mathbb{R}^n\setminus\{\mathbf{0}\}$ the notion $\widehat{\mathbf{x}}$ has to be understood as $\widehat{\mathbf{x}}:=\mathbf{x}/\|\mathbf{x}\|$.

Observing that $\widehat{\mathbf{n}}(\widehat{\mathbf{x}})=\widehat{\mathbf{x}}$ we can simplify the boundary parameterization (7) in accordance with

$$\boldsymbol{\gamma}:\mathbb{S}\to\Gamma,\quad \boldsymbol{\gamma}(\widehat{\mathbf{x}})=r(\widehat{\mathbf{x}})\cdot\widehat{\mathbf{x}}$$

Thus, observing the identities $\mathbf{V}(\mathbf{x})=\mathrm{d}r(\widehat{\mathbf{x}})\cdot\widehat{\mathbf{x}}$ and

$$\langle\mathbf{V},\mathbf{n}\rangle\,\mathrm{d}\sigma_{\mathbf{x}}=\mathrm{d}r(\widehat{\mathbf{x}})\langle\widehat{\mathbf{x}},\mathbf{n}\rangle\,\mathrm{d}\sigma_{\mathbf{x}}=\mathrm{d}r(\widehat{\mathbf{x}})r(\widehat{\mathbf{x}})^{n-1}\,\mathrm{d}\sigma_{\widehat{\mathbf{x}}}$$

one can rewrite the shape gradient (6) according to

$$\nabla J(r)[\mathrm{d}r]=\int_{\mathbb{S}}\mathrm{d}r r^{n-1}\left\{j(\boldsymbol{\gamma}(\widehat{\mathbf{x}}),g)+\frac{\partial p}{\partial\mathbf{n}}\frac{\partial(g-u)}{\partial\mathbf{n}}\right\}\mathrm{d}\sigma_{\widehat{\mathbf{x}}} \tag{9}$$

Therefore, in accordance with [10, 14], the boundary integral representation of the shape Hessian is given by

$$\begin{aligned}\nabla^2 J(r)[\mathrm{d}r_1,\mathrm{d}r_2]=\int_{\mathbb{S}}&\mathrm{d}r_1\mathrm{d}r_2 r^{n-2}(n-1)\left[j(\boldsymbol{\gamma}(\widehat{\mathbf{x}}),g)+\frac{\partial p}{\partial\mathbf{n}}\frac{\partial(g-u)}{\partial\mathbf{n}}\right]\\&+\mathrm{d}r_1\mathrm{d}r_2 r^{n-1}\frac{\partial}{\partial\widehat{\mathbf{x}}}\left[j(\boldsymbol{\gamma}(\widehat{\mathbf{x}}),g)+\frac{\partial p}{\partial\mathbf{n}}\frac{\partial(g-u)}{\partial\mathbf{n}}\right]\\&+\mathrm{d}r_1 r^{n-1}\left[\frac{\partial p}{\partial\mathbf{n}}\frac{\partial\mathrm{d}u[\mathrm{d}r_2]}{\partial\mathbf{n}}-\frac{\partial\mathrm{d}p[\mathrm{d}r_2]}{\partial\mathbf{n}}\frac{\partial(g-u)}{\partial\mathbf{n}}\right]\mathrm{d}\sigma_{\widehat{\mathbf{x}}}\end{aligned} \tag{10}$$

DOI: 10.1002/mma

Herein, the notion $\partial/\partial\widehat{\mathbf{x}}$ has to be understood in the sense of $\partial u/\partial\widehat{\mathbf{x}}=\langle\nabla u,\widehat{\mathbf{x}}\rangle$. Moreover, $\mathrm{d}u[\mathrm{d}r_2]$ and $\mathrm{d}p[\mathrm{d}r_2]$ denote the local shape derivatives of the state function and the adjoint state function, which satisfy the boundary value problems (4) and

$$\begin{aligned} -\Delta \mathrm{d}p[\mathrm{d}r_2] &= \mathrm{d}u[\mathrm{d}r_2]\cdot\frac{\partial^2 j}{\partial u^2}(\cdot,u) \quad \text{in } \Omega \\ \mathrm{d}p[\mathrm{d}r_2] &= -\mathrm{d}r_2\langle\widehat{\mathbf{x}},\mathbf{n}\rangle\frac{\partial p}{\partial\mathbf{n}} \quad \text{on } \Gamma \end{aligned} \tag{11}$$

respectively.

The first two terms in the boundary integral representation (10) of the shape Hessian are associated with a bilinear form on $L^2(\mathbb{S})\times L^2(\mathbb{S})$. The last term involves a Dirichlet-to-Neumann map of $\mathrm{d}r_2$ using (4) and (11). Consequently, as one readily verifies, the shape Hessian is a pseudo-differential operator of order $+1$, see also [15–17].

2.3. Necessary and sufficient optimality conditions

Recall that, by introducing a reference manifold and a fixed variation field, we embedded the shape calculus into the Banach space $X=C^{2,\alpha}(\mathbb{S})$. We shall now consider the minimization of the shape functional (1), that is

$$J(r)\to\min, \quad r\in X \tag{12}$$

Herein, $J:X\mapsto\mathbb{R}$ defines a two times continuously differentiable functional, i.e. the gradient $\nabla J(r)\in X^\star$ as well as the Hessian $\nabla^2 J(r)\in\mathscr{L}(X,X^\star)$ exist for all $r\in X$, and the mappings $\nabla J(\cdot):X\to X^\star$, $\nabla^2 J(\cdot):X\to\mathscr{L}(X,X^\star)$ are continuous. In fact, the shape Hessian is even Hölder continuous with exponent $\alpha>0$, cf. [18].

Theorem 2 (*Necessary first-order optimality condition*)
Let $r^\star$ be a regular optimal solution for problem (12), i.e. there exists $\delta>0$ such that

$$J(r^\star)<J(r) \quad \text{for all } \|r^\star-r\|_X<\delta$$

Then, there holds

$$\nabla J(r^\star)[\mathrm{d}r]=0 \quad \text{for all } \mathrm{d}r\in X \tag{13}$$

Let $r^\star$ be such that (13) holds that is, $r^\star$ is a *stationary domain* of problem (12). According to [18], we find the following Taylor expansion for all domains $r\in X$, described by $r=r^\star+\mathrm{d}r$, in the neighbourhood of $r^\star$

$$J(r)-J(r^\star)=0+\tfrac{1}{2}\nabla^2 J(r^\star)[\mathrm{d}r,\mathrm{d}r]+\eta(\|\mathrm{d}r\|_X) \tag{14}$$

Herein, the second-order Taylor remainder (cf. [18]) fulfills

$$|\eta(\|\mathrm{d}r\|_X)|=o(\|\mathrm{d}r\|_X)\|\mathrm{d}r\|^2_{H^{1/2}(\mathbb{S})} \tag{15}$$

The Taylor expansion (14) implies that $J(r^\star)$ is a regular local minimizer of second order if and only if $\nabla^2 J(r^\star)$ is *strictly* coercive. However, as the shape Hessian defines a pseudo-differential operator of order $+1$, we cannot expect coercivity of the shape Hessian in the Banach space X. Coercivity can be expected only in the weaker space $H^{1/2}(\mathbb{S})$.

DOI: 10.1002/mma

Theorem 3 (*Eppler et al.* [*17*])
The stationary domain $r^\star$ is a regular local minimizer of second order if and only if the shape Hessian is $H^{1/2}(\mathbb{S})$-coercive, that is

$$\nabla^2 J(r^\star)[\mathrm{d}r, \mathrm{d}r] \gtrsim \|\mathrm{d}r\|^2_{H^{1/2}(\mathbb{S})} \tag{16}$$

We emphasize that the radial function $r^\star$ has to be in X to ensure (14) and (15), while a minimizer is stable if the shape Hessian is $H^{1/2}(\mathbb{S})$-coercive. For more details on this phenomenon, called *two-norm discrepancy*, we refer to [17–20].

2.4. Free boundary problems—a class of well-posed problems

A bright class of generally well-posed shape optimization problems issues from free boundary problems. Let $T \subset \mathbb{R}^n$ denote a bounded domain with boundary $\partial T = \Gamma$. Inside the domain T we assume the existence of a simply connected subdomain $S \subset T$ with boundary $\partial S = \Sigma$. The resulting annular domain $T \setminus \overline{S}$ is denoted by Ω. Figure 1 refers to the given topological setup.

We consider the following overdetermined boundary value problem in the annular domain Ω

$$\begin{aligned} -\Delta u &= f \quad \text{in } \Omega \\ \|\nabla u\| &= g, \quad u = 0 \text{ on } \Gamma \\ u &= h \quad \text{on } \Sigma \end{aligned} \tag{17}$$

where $g, h > 0$ and $f \geqslant 0$ are sufficiently smooth functions.

We like to stress that the positivity of the Dirichlet data implies that u is positive in Ω. As, moreover, u admits homogeneous Dirichlet data on Γ, all tangential derivates of u along Γ are zero. Thus, the gradient has only a component in normal direction which leads to the identity

$$\|\nabla u\| \equiv -\frac{\partial u}{\partial \mathbf{n}} \quad \text{on } \Gamma$$

We arrive at a free boundary problem if the boundary Γ is the unknown. In other words, we seek a domain Ω with fixed boundary Σ and unknown boundary Γ such that the overdetermined boundary value problem (17) is solvable. For the existence of solutions of this generalized *exterior Bernoulli*

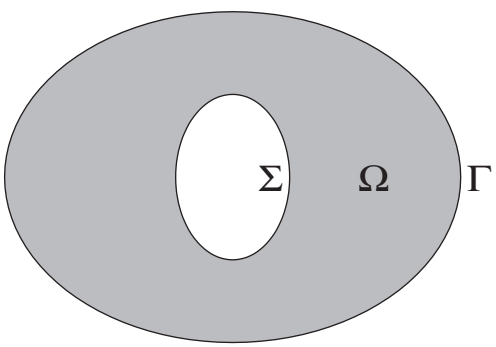

Figure 1. The domain Ω and its boundaries Γ and Σ.

DOI: 10.1002/mma

free boundary problem we refer the reader to, e.g. [5], see also [6] for the related *interior* free boundary problem. Results concerning the geometric form of the solutions can be found in e.g. [21] and the references therein.

Shape optimization provides an efficient tool to solve such free boundary value problems, cf. [4, 16, 22, 23]. We consider the cost functional

$$J(\Omega)=\int_{\Omega}\|\nabla u\|^2-2fu+g^2\,\mathrm{d}\mathbf{x} \tag{18}$$

with underlying state equation

$$\begin{aligned}-\Delta u &= f \quad \text{in } \Omega\\ u &= 0 \quad \text{on } \Gamma\\ u &= h \quad \text{on } \Sigma\end{aligned} \tag{19}$$

By virtue of the Gauss theorem we arrive at

$$J(\Omega)=\int_{\Omega}g^2-fu\,\mathrm{d}\mathbf{x}+\int_{\Sigma}\frac{\partial u}{\partial\mathbf{n}}h\,\mathrm{d}\sigma_{\mathbf{x}} \tag{20}$$

As the boundary Σ is fixed, we conclude

$$\nabla\left(\int_{\Sigma}\frac{\partial u}{\partial\mathbf{n}}h\,\mathrm{d}\sigma_{\mathbf{x}}\right)[\mathbf{V}]=\int_{\Sigma}\frac{\partial\,\mathrm{d}u[\mathbf{V}]}{\partial\mathbf{n}}h\,\mathrm{d}\sigma_{\mathbf{x}}$$

for any sufficiently smooth variation field $\mathbf{V}$. Thus, one finds that the first and second shape derivatives are given as in Sections 2.1 and 2.2, where the identity $p=-u$ holds. Consequently, the solution of the free boundary problem is equivalent to the shape optimization problem $J(\Omega)\to\min$ since the necessary condition of a minimizer of (18) reads as

$$\nabla J(\Omega)[\mathbf{V}]=\int_{\Gamma^\star}\langle\mathbf{V},\mathbf{n}\rangle\left\{g^2-\left[\frac{\partial u}{\partial\mathbf{n}}\right]^2\right\}\mathrm{d}\sigma_{\mathbf{x}}\overset{!}{=}0 \tag{21}$$

for all sufficiently smooth perturbation fields $\mathbf{V}$. In other words, via shape optimization a variational formulation of the condition

$$\frac{\partial u}{\partial\mathbf{n}}=-g\quad\text{on }\Gamma$$

is induced. At least under certain circumstances we can prove the coercivity of the shape Hessian at a stationary domain.

Theorem 4 (*Eppler and Harbrecht* [*16*])
Assume that $\Omega^\star$ is a stationary domain of the shape functional (18). Then, the shape Hessian is $H^{1/2}(\mathbb{S})$-coercive if

$$\kappa+\left[\frac{\partial g}{\partial\mathbf{n}}-f\right]\Big/g\geqslant 0\quad\text{on }\Gamma^\star$$

where κ (respectively $2\mathscr{H}$ if $n=3$) denotes the mean curvature. In particular, in the case $g\equiv\text{const.}$ and $f\equiv 0$, the shape Hessian is $H^{1/2}(\mathbb{S})$-coercive if the boundary $\Gamma^\star$ is convex (seen from inside).

DOI: 10.1002/mma

The problem under consideration can be viewed as the prototype of a free boundary problem arising in many applications. For example, the growth of anodes in electrochemical processing might be modeled like above with $f \equiv 0$ and $g, h \equiv 1$.

In the two-dimensional exterior magnetic shaping of liquid metals the state equation is an exterior Poisson equation and the uniqueness is ensured by a volume constraint of the domain Ω [7–9]. However, as the shape functional involves the perimeter, which corresponds to the surface tension of the liquid, the energy space of the shape Hessian will be $H^1(\mathbb{S})$.

Remark 5
The detection of voids or inclusions in electrical impedance tomography is slightly different as the roles of Σ and Γ are interchanged [15, 24]. Particularly, this inverse problem is severely ill-posed, in contrast to the present class of problems. It has been proven in [15] that the shape Hessian is *not* strictly coercive in any $H^s(\mathbb{S})$ for all $s \in \mathbb{R}$.

2.5. Compactly supported functionals—a class of ill-posed problems

Engineers often aim at designing the shape of the domain $\Omega \in \mathbb{R}^n$ of definition for the underlying boundary value problem such that the state achieves prescribed values in a fixed subregion $B \subset\subset \Omega$, see also Figure 2. Mathematically speaking, this leads to an objective of the type

$$J(\Omega) = \int_B j(u(\mathbf{x}), \mathbf{x})\, \mathrm{d}\mathbf{x} \to \min \tag{22}$$

where the state u satisfies the Poisson equation (2). In particular, for a given function u_d, the choice $j(u) = (u - u_d)^2$ yields the well-known $L^2(B)$-tracking functional. As the investigation of the stability of stationary domains will show, this class of shape optimization problems is severely ill-posed.

Extending the objective j by the trivial extension to the whole domain Ω the shape gradient and Hessian are given as in (6) and (10), respectively, where the adjoint state reads now as (cf. (5))

$$-\Delta p = \chi_B \cdot \frac{\partial j}{\partial u}(u(\cdot), \cdot) \ \text{ in } \Omega, \quad p = 0 \ \text{ on } \ \Gamma \tag{23}$$

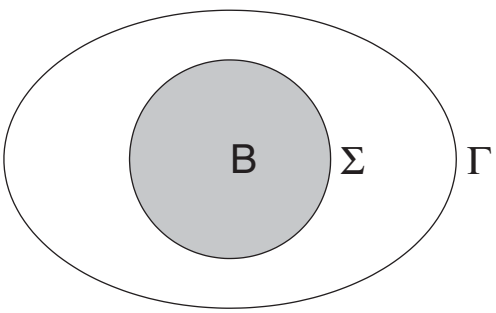

Figure 2. The domain Ω, the subdomain B, and the boundaries Γ and Σ.

DOI: 10.1002/mma

and correspondingly the adjoint local shape derivative as (cf. (11))

$$\begin{aligned} -\Delta \mathrm{d}p[\mathrm{d}r_2] &= \chi_B \cdot \mathrm{d}u[\mathrm{d}r_2] \frac{\partial^2 j}{\partial u^2}(u(\cdot),\cdot) \quad \text{in } \Omega \\ \mathrm{d}p[\mathrm{d}r_2] &= -\mathrm{d}r_2 \langle \widehat{\mathbf{x}}, \mathbf{n} \rangle \frac{\partial p}{\partial \mathbf{n}} \quad \text{on } \Gamma \end{aligned} \tag{24}$$

Herein, χ_B denotes the characteristic function of B, i.e. $\chi_B = 1$ on B and $\chi_B = 0$ on $\mathbb{R}^n \setminus B$.

In the non-degenerated case we have $\partial(g-u)/\partial \mathbf{n} \not\equiv 0$ on Γ. Therefore, the necessary condition implies $\partial p/\partial \mathbf{n} \equiv 0$ on $\Gamma^\star$ since p is harmonic in $\Omega^\star \setminus \overline{B}$, admitting homogeneous Dirichlet data at $\Gamma^\star$ (cf. [25]). Consequently, the shape Hessian (10) simplifies at a stationary domain to

$$\nabla^2 J(\Omega^\star)[\mathrm{d}r_1, \mathrm{d}r_2] = \int_{\mathbb{S}} \mathrm{d}r_1 r^{n-1} \frac{\partial \mathrm{d}p[\mathrm{d}r_2]}{\partial \mathbf{n}} \cdot \frac{\partial (g-u)}{\partial \mathbf{n}} \, \mathrm{d}\sigma_{\widehat{\mathbf{x}}} \tag{25}$$

In particular, the adjoint local shape derivative $\mathrm{d}p = \mathrm{d}p[\mathrm{d}r_2]$, defined in (24), admits homogeneous Dirichlet data. Since therefore the adjoint local shape derivative and thus its Neumann data $\partial \mathrm{d}p[\mathrm{d}r_2]/\partial \mathbf{n}$ depend only on data living on B and $\mathrm{dist}(B, \Gamma^\star) > 0$, the shape Hessian (25) is compact.

Theorem 6 (*Eppler and Harbrecht* [25])
Assume that $\Omega^\star$ is a stationary solution of the shape functional (22). Then, the shape Hessian at $\Omega^\star$ defines a compact mapping $\nabla^2 J(\Omega^\star) : H^{1/2}(\Gamma) \to H^{-1/2}(\Gamma)$. It defines even an arbitrarily smoothing pseudo-differential operator if $\Omega^\star \in C^\infty$.

Remark 7
Note that, since tracking-type functionals allow a reinterpretation as inverse problems (see, e.g. [26]), the compactness of the shape Hessian at the minimizing domain refers directly to the ill-posedness of the underlying identification problem.

3. SHAPE APPROXIMATION

3.1. Non-linear Ritz–Galerkin approximation

In order to solve the minimization problem defined by (1) and (2), we are seeking the stationary points $r^\star \in X$ satisfying

$$\nabla J(r^\star)[\mathrm{d}r] = 0 \quad \text{for all } \mathrm{d}r \in X \tag{26}$$

In accordance with [17] we shall introduce a Ritz–Galerkin method for the non-linear equation (26). To this end, we restrict ourselves again to star-shaped domains and consider the gradient in terms of spherical coordinates (9). Nevertheless, one can consider any fixed variation field with respect to a smooth reference manifold as well.

Let $\varphi_i : \mathbb{S} \to \mathbb{R}$ denote suitable ansatz functions and consider the ansatz space

$$V_N = \mathrm{span}\{\varphi_1, \varphi_2, \ldots, \varphi_N\} \subset X \tag{27}$$

In practice, we will use the first N spherical harmonics in $\mathbb{R}^n$ as ansatz functions.

DOI: 10.1002/mma

We now replace (26) by its finite dimensional counterpart:

$$\text{seek } r_N^\star \in V_N \text{ such that } \quad \nabla J(r_N^\star)[\mathrm{d}r] = 0 \text{ for all } \mathrm{d}r \in V_N \tag{28}$$

Note that this is the necessary condition associated with the finite dimensional optimization problem

$$J(r_N) \to \min, \quad r_N \in V_N \tag{29}$$

Concerning the existence and convergence of approximate shapes we have the following theorem.

Theorem 8 (*Eppler et al.* [*17*])
Assume that the shape Hessian is strictly $H^{1/2}(\mathbb{S})$-coercive at the stationary domain $r^\star \in X$. Then, (29) admits a unique solution $r_N^\star \in V_N$ provided that N is large enough. The approximation error stays in the energy norm proportional to the best approximation in V_N, that is

$$\|r_N^\star - r^\star\|_{H^{1/2}(\mathbb{S})} \lesssim \inf_{r_N \in V_N} \|r_N - r^\star\|_{H^{1/2}(\mathbb{S})}$$

Of course, from this theorem one can compute the *rate of convergence* by estimating $\inf_{r_N \in V_N} \|r_N - r^\star\|_{H^{1/2}(\mathbb{S})}$.

Different strategies exist to find $r_N \in V_N$ such that (28) holds. In general, one makes the ansatz $r_N = \sum_{i=1}^N r_i \varphi_i$ and considers the iterative scheme

$$\mathbf{r}^{(n+1)} = \mathbf{r}^{(n)} - h^{(n)} \mathbf{M}^{(n)} \mathbf{G}^{(n)}, \quad n = 0, 1, 2, \ldots \tag{30}$$

where $h^{(n)}$ is a suitable step width and

$$\mathbf{r}^{(n)} = (r_i^{(n)})_{i=1,\ldots,N}, \quad \mathbf{G}^{(n)} := (\nabla J(r_N^{(n)})[\varphi_i])_{i=1,\ldots,N}$$

First-order methods are the gradient method ($\mathbf{M}^{(n)} := \mathbf{I}$) or the quasi-Newton method where $\mathbf{M}^{(n)}$ denotes a suitable approximation to the inverse shape Hessian. Choosing

$$\mathbf{M}^{(n)} := (\nabla^2 J(r_N^{(n)})[\varphi_i, \varphi_j])_{i,j=1,\ldots,N}^{-1}$$

we arrive at the Newton method, which converges much faster compared with the first-order methods, see [27], for example. For a survey on available optimization algorithms we refer the reader to [28, 29].

The following statement is an immediate consequence of Theorem 8.

Corollary 9 (*Eppler and Harbrecht* [*16*])
Under the assumptions of Theorem 8 the iterants $r_N^{(n)}$ produced by algorithm (30) converge to $r_N^\star$ provided that the initial guess $r_N^{(0)}$ is properly chosen.

3.2. More flexible boundary representations

If one intends to implement only first-order shape optimization algorithms, one may employ a more general boundary representation than the restrictive approach (7), (8).

The boundary of a domain Ω can be represented by a bijective positive-oriented function

$$\boldsymbol{\gamma}: \mathbb{S} \to \Gamma, \quad \boldsymbol{\gamma}(\widehat{\mathbf{x}}) = [\gamma_1(\widehat{\mathbf{x}}), \ldots, \gamma_n(\widehat{\mathbf{x}})]^{\mathrm{T}} \tag{31}$$

DOI: 10.1002/mma

such that $\gamma_1, \ldots, \gamma_n \in C^2(\mathbb{S})$. Consider again the ansatz space V_N from (27). To discretize the shape optimization problem we make this time the ansatz

$$\boldsymbol{\gamma}_N = \sum_{k=-N}^{N} \mathbf{a}_k \varphi_k \in V_N^n \tag{32}$$

with *vector-valued* coefficients $\mathbf{a}_k \in \mathbb{R}^n$.

On the one hand, ansatz (32) does not impose any restriction to the topology of the domain except for its genus. On the other hand, the parametric representation (31) of the domain Ω is not unique. In fact, if $\Xi : \mathbb{S} \to \mathbb{S}$ denotes any smooth bijective mapping, then the function $\boldsymbol{\gamma} \circ \Xi$ describes another parametrization of Ω. Consequently, one cannot expect convergence results similar to that of Theorem 8.

To avoid degenerated boundary representations one can apply from time to time a suitable remeshing algorithm. However, even for a large number of degrees of freedom, the surface, and thus the value of the cost functional, is changed considerably by remeshing. Consequently, it might happen that the shape optimization algorithm does not converge. To our experience it is preferable to regularize the shape functional instead. It is quite obvious that, for numerical computations, a 'nice' parametrization maps orthonormal tangents $\{\mathbf{t}_i\}_{i=1}^n$ on the parameter space $\mathbb{S}$ to orthogonal tangents on the boundary Γ, possibly with the same length on whole Γ. Therefore, we consider the mesh functional

$$M(\Omega) = \int_{\mathbb{S}} \left\| \mathscr{T}(\widehat{\mathbf{x}}) - \left(\frac{|\Gamma|}{|\mathbb{S}|} \right)^{2/n-1} \mathbf{I} \right\|_F^2 \mathrm{d}\sigma_{\widehat{\mathbf{x}}}$$

where $\mathscr{T}$ is the first fundamental tensor of differential geometry, given by

$$\mathscr{T}(\widehat{\mathbf{x}}) = \left[\left\langle \frac{\partial \boldsymbol{\gamma}(\widehat{\mathbf{x}})}{\partial \mathbf{t}_i}, \frac{\partial \boldsymbol{\gamma}(\widehat{\mathbf{x}})}{\partial \mathbf{t}_j} \right\rangle \right]_{i,j=1}^{n-1}$$

and $\|\cdot\|_F$ denotes the Frobenius norm. The mesh functional is identical to zero if and only if the above claim is fulfilled. This motivates to solve for small $\beta > 0$ the *regularized* shape problem

$$J(\Omega) + \beta M(\Omega) \to \min_{\Omega \in \Upsilon}$$

instead of the original problem (1). It is well known that the best results are achieved when $\beta \to 0$ during the optimization procedure, see also [30].

3.3. Computing domain integrals

Boundary integrals can be computed by employing the parametric representation of the boundary. However, the evaluation of domain integrals

$$I(\Omega) := \int_{\Omega} f(\mathbf{x}) \, \mathrm{d}\mathbf{x} \tag{33}$$

where $f \in C(\overline{\Omega})$, requires a suitable triangulation of the domain. For two space dimensions such a triangulation can be constructed as follows.

DOI: 10.1002/mma

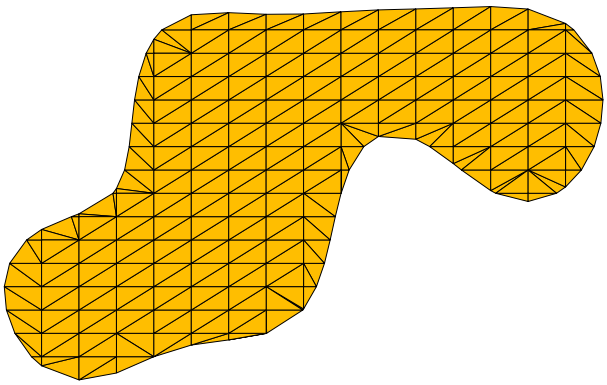

Figure 3. Triangulation of the domain.

We compute the points of intersection of the boundary curve Γ and the grid $\bigcup_{\mathbf{k}\in\mathbb{Z}^2}\partial Q_{j,\mathbf{k}}$, generated from the squares

$$Q_{j,\mathbf{k}}:=[2^{-j}k_1,2^{-j}(k_1+1)]\times[2^{-j}k_2,2^{-j}(k_2+1)]$$

Then, we replace the boundary curve Γ by the piecewise linear curve $\widetilde{\Gamma}$ which connects these points by straight lines. The enclosed polygonal domain will be denoted by $\widetilde{\Omega}$.

We will next construct a suitable triangulation of $\widetilde{\Omega}$. We subdivide all elements $Q_{j,\mathbf{k}}$ that intersect the boundary $\widetilde{\Gamma}$ into suitable triangles to triangulate $Q_{j,\mathbf{k}}\cap\widetilde{\Omega}$. In the remaining part of $\widetilde{\Omega}$ we subdivide the elements $Q_{j,\mathbf{k}}$ into two triangles. Finally, we apply appropriate quadrature formulae on triangles. Figure 3 exemplifies a triangulation produced by our algorithm. Of course, there may appear also rather degenerated triangles. However, in connection with numerical quadrature, this does not matter.

In complete analogy one introduces in the three-dimensional case a triangulation of the free surface and henceforth a tetrahedral mesh of the domain.

Theorem 10 (*Eppler et al.* [*30*])
Assume that $\Omega\in C^2$ and $f\in C^2(\mathbb{D})$. Then the above quadrature algorithm computes the integral $I(\Omega)$ from (33) with accuracy $\mathcal{O}(h_j^2)$, where $h_j=2^{-j}$, provided that the element quadrature formulae are exact for linear polynomials.

4. SOLVING THE STATE EQUATION

4.1. Boundary element methods

In order to compute shape gradients and Hessians one only needs boundary values of the underlying state and adjoint state functions. However, the evaluation of the cost functional (1) seems to require the explicit knowledge of the state u on the complete domain Ω. At least in the case of free boundary problems this is not the case.

Thanks to a suitable Newton potential the functional (18) as well as its gradient and Hessian can be derived from the boundary data of a harmonic function. Thus, the use of boundary integral

DOI: 10.1002/mma

equations is highly attractive since their numerical solution requires only a triangulation of the boundary. That way, large domain deformations become realizable without remeshing as necessary, for example, when using FEMs. Additionally, compared with FEMs, the complexity is even reduced if we apply modern BEMs such as, e.g. the *multipole method* [31], $\mathscr{H}$*-matrices* [32] or the *wavelet Galerkin scheme* [33].

We shall now introduce the Newton potential N_f that satisfies

$$-\Delta N_f = f \quad \text{in } \Omega \tag{34}$$

This Newton potential is supposed to be explicitly known or computed once with sufficiently high accuracy. Since both, the computational domain $\widehat{\Omega}$ and the boundary conditions, can be chosen arbitrary, efficient solution techniques can be used without further difficulties. For a particular realization, see, e.g. [34].

Via the ansatz

$$u = N_f + v \tag{35}$$

the state equation (19) is transformed to the following Dirichlet problem for the Laplacian:

$$\begin{aligned} \Delta v &= 0 \quad \text{in } \Omega \\ v &= -N_f \quad \text{on } \Gamma \\ v &= h - N_f \quad \text{on } \Sigma \end{aligned} \tag{36}$$

To reformulate the cost functional (18) we apply integration by parts (cf. (20))

$$J(\Omega) = \int_\Omega \|\nabla u\|^2 - 2fu + g^2 \,\mathrm{d}\mathbf{x} = \int_\Omega g^2 - (N_f + v) f \,\mathrm{d}\mathbf{x} + \int_\Sigma \frac{\partial (N_f + v)}{\partial \mathbf{n}} h \,\mathrm{d}\sigma_\mathbf{x} \tag{37}$$

Green's second formula implies the identity

$$\int_\Omega vf \,\mathrm{d}\mathbf{x} = \int_{\partial\Omega} \frac{\partial v}{\partial \mathbf{n}} N_f \,\mathrm{d}\sigma_\mathbf{x} - \int_{\partial\Omega} v \frac{\partial N_f}{\partial \mathbf{n}} \,\mathrm{d}\sigma_\mathbf{x} = \int_{\partial\Omega} N_f \frac{\partial u}{\partial \mathbf{n}} \,\mathrm{d}\sigma_\mathbf{x} - \int_\Sigma h \frac{\partial N_f}{\partial \mathbf{n}} \,\mathrm{d}\sigma_\mathbf{x}$$

Inserting this equation into (37) gives

$$J(\Omega) = \int_\Omega g^2 - N_f f \,\mathrm{d}\mathbf{x} + \int_\Sigma \frac{\partial (2N_f + v)}{\partial \mathbf{n}} h \,\mathrm{d}\sigma_\mathbf{x} - \int_{\partial\Omega} N_f \frac{\partial u}{\partial \mathbf{n}} \,\mathrm{d}\sigma_\mathbf{x} \tag{38}$$

Consequently, both the cost functional and its gradient (cf. (21)) can be computed provided that the normal derivative $\partial u / \partial \mathbf{n}$ is known. Its knowledge is therefore sufficient to perform a first-order optimization method. Recall that the remaining domain integral in (38) can be computed according to Section 3.3.

Ansatz (35) leads to the normal derivative $\partial u / \partial \mathbf{n}$ according to

$$\frac{\partial u}{\partial \mathbf{n}} = \frac{\partial v}{\partial \mathbf{n}} + \frac{\partial N_f}{\partial \mathbf{n}}$$

DOI: 10.1002/mma

with the Newton potential N_f defined via (34) and v satisfying the boundary value problem (36). We introduce the *single-layer operator* $\mathscr{V}$ and the *double-layer operator* $\mathscr{K}$ defined by

$$\begin{aligned}(\mathscr{V}u)(\mathbf{x}) &:= \int_{\partial\Omega} E(\mathbf{x},\mathbf{y})u(\mathbf{y})\,\mathrm{d}\sigma_{\mathbf{y}} \\ (\mathscr{K}u)(\mathbf{x}) &:= \int_{\partial\Omega} \frac{\partial E(\mathbf{x},\mathbf{y})}{\partial \mathbf{n}(\mathbf{y})} u(\mathbf{y})\,\mathrm{d}\sigma_{\mathbf{y}}\end{aligned}, \quad \mathbf{x}\in\partial\Omega$$

where the fundamental solution $E(\mathbf{x},\mathbf{y})$ of the Laplacian is given by

$$E(\mathbf{x},\mathbf{y}) := \begin{cases} -\dfrac{1}{2\pi}\log\|\mathbf{x}-\mathbf{y}\| & \text{if } n=2 \\ \dfrac{1}{4\pi}\dfrac{1}{\|\mathbf{x}-\mathbf{y}\|} & \text{if } n=3 \end{cases} \tag{39}$$

Thus, the normal derivative of v is derived by the following boundary integral equation, the so-called *Dirichlet-to-Neumann map*:

$$\mathscr{V}\frac{\partial v}{\partial \mathbf{n}} = \left(\frac{1}{2}+\mathscr{K}\right)(h\chi_\Sigma - N_f) \tag{40}$$

Remark 11
Via BEMs also second-order derivatives of the state function, as required for the shape Hessian, become computable and thus a Newton method can be realized. For the sake of brevity we skip the details and refer the reader to [16, 27] for details.

4.2. Coupling of FEMs and BEMs

In difference to the previous subsection the adjoint state depends directly on the state if we consider compactly supported shape functionals. Fortunately, the coupling of FEMs and BEMs will essentially retain all the structural and computational advantages of treating the free boundary by boundary integral equations.

Let $\Omega\in\mathbb{R}^n$, $n=2,3$, be a simply connected domain with boundary $\Gamma:=\partial\Omega$ and assume a fixed subdomain $B\subset\Omega$, see also Figure 2. Consider the shape optimization problem (22), where the state u satisfies the Poisson equation (2). The adjoint state function p, involved in the shape gradient (6), satisfies the boundary value problem (23). Thus, the adjoint state depends on the actual state u. Consequently, a numerical method for solving the state equation (2) should provide a fast access to u in the set B, such as FEMs. However, we like to preserve the advantages of BEMs to treat the free boundary Γ. This suggests to couple FEMs and BEMs in order to compute the state and its adjoint.

We consider again the Newton potential (34) to resolve the inhomogeneity of the state equation (2) by ansatz (35). Consequently, in view of the adjoint state equation (23), it suffices to consider a numerical method to solve

$$\begin{aligned} -\Delta v &= f \quad \text{in } B \\ \Delta v &= 0 \quad \text{in } \Omega\setminus\overline{B} \\ v &= g \quad \text{on } \Gamma \end{aligned} \tag{41}$$

DOI: 10.1002/mma

We set $\Sigma := \partial B$ and assume the normal vectors $\mathbf{n}$ at Γ and Σ to point into $\Omega \setminus \overline{B}$, cf. Figure 2 for the topological situation. Then, (41) can be split into the following two coupled boundary value problems

$$\begin{aligned} &-\Delta v = f \ \text{ in } B, \quad \Delta v = 0 \ \text{ on } \Omega \setminus \overline{B}, \quad v = g \ \text{ on } \Gamma \\ &\lim_{\substack{\mathbf{y}\to\mathbf{x}\\ \mathbf{y}\in B}} v(\mathbf{y}) = \lim_{\substack{\mathbf{y}\to\mathbf{x}\\ \mathbf{y}\in\Omega\setminus\overline{B}}} v(\mathbf{y}), \quad \lim_{\substack{\mathbf{y}\to\mathbf{x}\\ \mathbf{y}\in B}} \frac{\partial v}{\partial \mathbf{n}}(\mathbf{y}) = \lim_{\substack{\mathbf{y}\to\mathbf{x}\\ \mathbf{y}\in\Omega\setminus\overline{B}}} \frac{\partial v}{\partial \mathbf{n}}(\mathbf{y}) \ \text{ for all } \mathbf{x}\in\Sigma \end{aligned} \tag{42}$$

We introduce the *single-layer operator* $\mathscr{V}_{\Phi\Psi}$, the *double-layer operator* $\mathscr{K}_{\Phi\Psi}$, the *adjoint double-layer operator* $\mathscr{K}^{\star}_{\Psi\Phi}$ and the *hypersingular operator* $\mathscr{W}_{\Phi\Psi}$ with respect to the boundaries $\Phi, \Psi \in \{\Gamma, \Sigma\}$ by

$$\begin{aligned} (\mathscr{V}_{\Phi\Psi}u)(\mathbf{x}) &:= \int_{\Phi} E(\mathbf{x},\mathbf{y})u(\mathbf{y})\,\mathrm{d}\sigma_{\mathbf{y}} \\ (\mathscr{K}_{\Phi\Psi}u)(\mathbf{x}) &:= \int_{\Phi} \frac{\partial E(\mathbf{x},\mathbf{y})}{\partial \mathbf{n}(\mathbf{y})}u(\mathbf{y})\,\mathrm{d}\sigma_{\mathbf{y}} \\ (\mathscr{K}^{\star}_{\Phi\Psi}u)(\mathbf{x}) &:= \int_{\Phi} \frac{\partial}{\partial \mathbf{n}(\mathbf{x})}E(\mathbf{x},\mathbf{y})u(\mathbf{y})\,\mathrm{d}\sigma_{\mathbf{y}} \\ (\mathscr{W}_{\Phi\Psi}u)(\mathbf{x}) &:= -\frac{\partial}{\partial \mathbf{n}(\mathbf{x})}\int_{\Phi} \frac{\partial E(\mathbf{x},\mathbf{y})}{\partial \mathbf{n}(\mathbf{y})}u(\mathbf{y})\,\mathrm{d}\sigma_{\mathbf{y}} \end{aligned} \quad , \quad \mathbf{x}\in\Psi$$

where the fundamental solution $E(\mathbf{x},\mathbf{y})$ is defined as in (39).

Finally, introducing the variables $\sigma_\Sigma := (\partial v/\partial \mathbf{n})|_\Sigma$ and $\sigma_\Gamma := (\partial v/\partial \mathbf{n})|_\Gamma$, the coupled system (42) yields the following non-local boundary value problem:

Find $(v, \sigma_\Sigma, \sigma_\Gamma) \in H^1(B) \times H^{-1/2}(\Sigma) \times H^{-1/2}(\Gamma)$ such that

$$\begin{aligned} &-\Delta v = f \ \text{ in } B, \quad \Delta v = 0 \ \text{ on } \Omega\setminus\overline{B} \\ &-\mathscr{W}_{\Sigma\Sigma}v - \mathscr{W}_{\Gamma\Sigma}g + \left(\tfrac{1}{2} - \mathscr{K}^{\star}_{\Sigma\Sigma}\right)\sigma_\Sigma - \mathscr{K}^{\star}_{\Gamma\Sigma}\sigma_\Gamma = \sigma_\Sigma \quad \text{on } \Sigma \\ &\left(\tfrac{1}{2} - \mathscr{K}_{\Sigma\Sigma}\right)v - \mathscr{K}_{\Gamma\Sigma}g + \mathscr{V}_{\Sigma\Sigma}\sigma_\Sigma + \mathscr{V}_{\Gamma\Sigma}\sigma_\Gamma = 0 \quad \text{on } \Sigma \\ &-\mathscr{K}_{\Sigma\Gamma}v + \left(\tfrac{1}{2} - \mathscr{K}_{\Gamma\Gamma}\right)g + \mathscr{V}_{\Sigma\Gamma}\sigma_\Sigma + \mathscr{V}_{\Gamma\Gamma}\sigma_\Gamma = 0 \quad \text{on } \Gamma \end{aligned} \tag{43}$$

This system is the so-called *two-integral formulation*, which is equivalent to our original model problem (41), see, for example, [35, 36].

The non-local boundary value problem (43) can be solved, e.g. along the lines of [37, 38]. Finite elements are applied to discretize the Poisson equation on B. The system matrices arising from the boundary integral operators are discretized by suitable wavelet bases. That way, applying wavelet matrix compression, the complexity is reduced (cf. [37]) and optimal preconditioners are available (cf. [38]). We refer the reader to [25] for details concerning our actual realization.

4.3. Fictitious domain methods

The above-mentioned techniques are not applicable to general shape functionals or to state equations that involve elliptic differential operators with non-constant coefficients. FDMs offer a convenient

DOI: 10.1002/mma

tool to deal with such shape optimization problems while the complicated remeshing, required for FEMs, is still avoided. We refer the reader to, e.g. [1, 39–41] for FDM in shape optimization.

To solve a boundary value problem with FDM, one embeds the *intrinsic domain* into a larger, but much simpler, *fictitious domain* (FD) $\mathbb{T}$, for example, a periodic n-cube. The next step is to construct from the original problem some auxiliary problem on the FD such that the solutions of this auxiliary and the original problem coincide on the intrinsic domain.

However, the success of FDM was limited since traditional methods suffer from low orders of convergence. For instance, the FD–Lagrange multiplier approach converges only as $\mathcal{O}(h^{1/2})$ in the energy norm when approximating from uniform grids with mesh size h (see [42]). Even adaptive schemes cannot overcome this restriction: the rate of convergence of standard (i.e. based on isotropic refinements) adaptive methods is limited by $\mathcal{O}(N^{-1/2})$ and $\mathcal{O}(N^{-1/4})$ in two and three spatial dimensions, respectively, when spending N degrees of freedom, independently of the order of the approximation spaces (see [43] for a more detailed discussion).

These difficulties arise from non-smooth extensions of the solution to the outside of the intrinsic domain. In particular, the approximation near the boundary is rather poor. Unfortunately, exactly the boundary data are the relevant data that enter the shape derivatives.

In [43, 44] a rather novel and promising *smoothness-preserving* FD (SPFD) method has been proposed which realizes higher orders of convergence due to smooth extensions of the solution. The capability of this method in the context of shape optimization problems has been demonstrated [30].

Consider the state equation (2), possibly with the more general elliptic differential operator $A: H^2(\mathbb{T}) \to L^2(\mathbb{T})$ instead of $-\Delta$, and assume the right-hand side f to be in $L^2(\mathbb{T})$. Then, since the boundary Γ is C^2, the solution of the state equation will be in $H^2(\Omega)$. The crucial idea of the SPFD method is to start with the following least-squares functional on $H^2(\mathbb{T})$: find $u^+ \in H^2(\mathbb{T})$ such that

$$\Phi(u^+) = \|P(Au^+ - f)\|^2_{L^2(\mathbb{T})} + \|u^+|_\Gamma - g\|^2_{H^{3/2}(\Gamma)} \to \min \tag{44}$$

where $P: L^2(\mathbb{T}) \to L^2(\mathbb{T})$ is such that Pv is the extension by zero of the restriction to Ω of $v \in L^2(\mathbb{T})$. Applying a suitable discretization, the approximate solution to (44) seems to be in fact smooth, as the numerical results in [30, 43] indicate. However, a strict proof is only available under additional assumptions, see [43, 44] for the details.

4.4. Finite element methods

Finite element discretizations require a suitable triangulation of the *varying* domain. To apply efficient solution techniques such as multigrid methods one needs a sequence of nested trial spaces. Such sequences can easily be defined if the given triangulation is nested.

On curved domains one can construct nested meshes via parameterization. We shall assume that the domain Ω is given as a collection of smooth patches. More precisely, let $\square := [0,1]^n$ denote the unit n-cube. The domain $\Omega \in \mathbb{R}^n$ is partitioned into a finite number of *patches*

$$\overline{\Omega} = \bigcup_{i=1}^{M} \Omega_i, \quad \Omega_i = \boldsymbol{\kappa}_i(\square), \quad i = 1, 2, \ldots, M$$

where each $\boldsymbol{\kappa}_i : \square \to \Omega_i$ defines a diffeomorphism of $\square$ onto Ω_i. The intersection $\Omega_i \cap \Omega_j$, $i \neq j$, of the patches Ω_i and Ω_j is supposed to be either $\emptyset$ or a lower-dimensional face.

A mesh of level j on Ω is induced by dyadic subdivisions of depth j of the unit cube into 2^{nj} cubes. This generates $2^{nj} M$ *elements* (or elementary domains). In order to ensure that the collection

DOI: 10.1002/mma

of elements on the level j forms a regular mesh on Ω, the parametric representation is subjected to the following *matching condition*: For all $\mathbf{y}\in\Omega_i\cap\Omega_j$ exists a bijective, affine mapping $\Xi:\square\to\square$ such that $\boldsymbol{\kappa}_i(\mathbf{x})=(\boldsymbol{\kappa}_j\circ\Xi)(\mathbf{x})=\mathbf{y}$ for $\mathbf{x}\in\square$ with $\boldsymbol{\kappa}_i(\mathbf{x})=\mathbf{y}$. We refer to Figure 5 for corresponding meshes on level $j=4$ consisting of $M=5$ patches.

For shape optimization we need meshes for the varying domain Ω. At least for small domain variations one can map a nested triangulation of a reference domain $\widehat{\Omega}$ via a piecewise smooth diffeomorphism to the actual domain Ω. For example, in case of ansatz (7), (8), having a parameterization $\{\widehat{\boldsymbol{\kappa}}_i\}$ of $\widehat{\Omega}$ in the above spirit at hand, smooth mappings $\Theta_i=\Theta_i(r)$ can be constructed such that $\Omega=\Omega(r)$ has the representation

$$\overline{\Omega}=\bigcup_{i=1}^{M}\Omega_i,\quad \Omega_i=\boldsymbol{\kappa}_i(\square)=(\Theta_i\circ\widehat{\boldsymbol{\kappa}}_i)(\square),\quad i=1,2,\ldots,M$$

where the matching condition still holds. That way, we will obtain a hierarchy on meshes on the domain Ω.

For illustrational reasons we shall consider two spatial dimensions and star-shaped domains, i.e. the unit circle as reference domain $\widehat{\Omega}$. In this case we are even able to construct directly the parameterization $\{\boldsymbol{\kappa}_i\}$ of the domain Ω. To that end, we assume the parameterization $\boldsymbol{\gamma}$ (31) to be defined as 2π-periodic function on the interval $[0,2\pi]$. Then, for arbitrary values $0\leqslant s<t\leqslant 2\pi$, the map

$$\boldsymbol{\kappa}_{i,1}(x,y)=\frac{1+y}{2}\cdot\boldsymbol{\gamma}(xs+(1-x)t),\quad (x,y)\in\square$$

defines a curved patch where one edge coincides with the piece $\boldsymbol{\gamma}([s,t])$ of the boundary curve Γ, see the left plot of Figure 4. A quadrilateral patch that connects the four endpoints of the latter curved one is given by

$$\boldsymbol{\kappa}_{i,2}(x,y)=\frac{(1+y)}{2}\{(1-x)\boldsymbol{\gamma}(t)+x\boldsymbol{\gamma}(s)\},\quad (x,y)\in\square$$

Combining both mappings according to

$$\boldsymbol{\gamma}_i(x,y)=y\cdot\boldsymbol{\kappa}_{i,1}(x,y)+(1-y)\cdot\boldsymbol{\kappa}_{i,2}(x,y),\quad (x,y)\in\square$$

leads to the final curved patch whose first edge coincides with Γ while the other edges are straight lines. That way, one can easily construct the parametric representation of the domain.

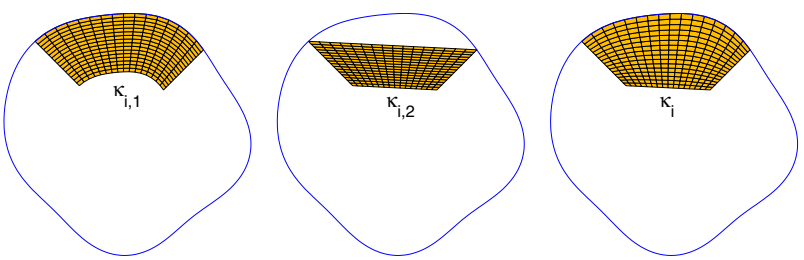

Figure 4. The images of the diffeomorphisms $\boldsymbol{\kappa}_{i,1}$ and $\boldsymbol{\kappa}_{i,2}$ and the final patch.

DOI: 10.1002/mma

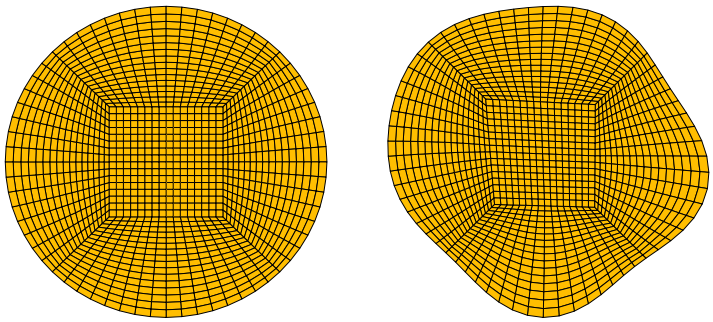

Figure 5. The quadrilateral mesh of the reference domain $\mathbb{S}$ and the domain Ω.

A visualization of the final mesh on level $j=4$ of the unit circle and the domain Ω is found in Figure 5. The present construction can be extended to general reference domains and to higher dimensions. Similar constructions are realizable in case of simplicial meshes.

Finally, we can define the ansatz functions via parametrization, lifting, for example, Lagrangian finite elements from $\square$ by using the mappings $\boldsymbol{\kappa}_i$ and gluing across patch boundaries. This yields the promised sequence of nested trial spaces. Thus, the efficient numerical solution of boundary value problems on Ω by multigrid schemes will be straightforward, see, e.g. [45–47].

REFERENCES

1. Haslinger J, Neitaanmäki P. *Finite Element Approximation for Optimal Shape*, *Material and Topology Design* (2nd edn). Wiley: Chichester, 1996.
2. Khludnev AM, Sokołowski J. *Modelling and Control in Solid Mechanics*. Birkhäuser: Basel, 1997.
3. Pironneau O. *Optimal Shape Design for Elliptic Systems*. Springer: New York, 1983.
4. Sokolowski J, Zolesio J-P. *Introduction to Shape Optimization*. Springer: Berlin, 1992.
5. Alt HW, Caffarelli LA. Existence and regularity for a minimum problem with free boundary. *Journal für Reine und Angewandte Mathematik* 1981; **325**:105–144.
6. Flucher M, Rumpf M. Bernoulli's free-boundary problem, qualitative theory and numerical approximation. *Journal für Reine und Angewandte Mathematik* 1997; **486**:165–204.
7. Colaud O, Henrot A. Numerical approximation of a free boundary problem arising in electromagnetic shaping. *SIAM Journal on Numerical Analysis* 1994; **31**:1109–1127.
8. Eppler K, Harbrecht H. Exterior electromagnetic shaping using wavelet BEM. *Mathematical Methods in the Applied Sciences* 2005; **28**:387–405.
9. Pierre M, Roche J-R. Computation of free surfaces in the electromagnetic shaping of liquid metals by optimization algorithms. *European Journal of Mechanics*, *B/Fluids* 1991; **10**:489–500.
10. Eppler K. Optimal shape design for elliptic equations via BIE-methods. *Journal of Applied Mathematics and Computer Science* 2000; **10**:487–516.
11. Kirsch A. The domain derivative and two applications in inverse scattering theory. *Inverse Problems* 1993; **9**:81–96.
12. Potthast R. Fréchet-Differenzierbarkeit von Randintegraloperatoren und Randwertproblemen zur Helmholtzgleichung und den zeitharmonischen Maxwellgleichungen. *Ph.D. Thesis*, Universität Göttingen, 1994.
13. Hadamard J. *Lessons on Calculus of Variations*. Gauthier-Villairs: Paris, 1910.
14. Eppler K. Boundary integral representations of second derivatives in shape optimization. *Discussiones Mathematicae* (*Differential Inclusion Control and Optimization*) 2000; **20**:63–78.

DOI: 10.1002/mma

15. Eppler K, Harbrecht H. A regularized Newton method in electrical impedance tomography using shape Hessian information. *Control and Cybernetics* 2005; **34**:203–225.
16. Eppler K, Harbrecht H. Efficient treatment of stationary free boundary problems. *Applied Numerical Mathematics* 2006; **56**:1326–1339.
17. Eppler K, Harbrecht H, Schneider R. On convergence in elliptic shape optimization. *SIAM Journal on Control and Optimization* 2007; **45**:61–83.
18. Dambrine M. On variations of the shape Hessian and sufficient conditions for the stability of critical shapes. *RACSAM*, *Revista de la Real Academia de Ciencias*, *Series A of Mathematics* 2002; **96**:95–121.
19. Dambrine M, Pierre M. About stability of equilibrium shapes. *M2AN*: *Mathematical Modeling and Numerical Analysis* 2000; **34**:811–834.
20. Eppler K. Second derivatives and sufficient optimality conditions for shape functionals. *Control and Cybernetics* 2000; **29**:485–512.
21. Acker A. On the geometric form of Bernoulli configurations. *Mathematical Methods in the Applied Sciences* 1988; **10**:1–14.
22. Delfour M, Zolesio J-P. *Shapes and Geometries*. SIAM: Philadelphia, PA, 2001.
23. Haslinger J, Kozubek T, Kunisch K, Peichl G. Shape optimization and fictitious domain approach for solving free boundary value problems of Bernoulli type. *Computational Optimization and Applications* 2003; **26**:231–251.
24. Roche J-R, Sokolowski J. Numerical methods for shape identification problems. *Control and Cybernetics* 1996; **25**:867–894.
25. Eppler K, Harbrecht H. Coupling of FEM and BEM in shape optimization. *Numerische Mathematik* 2006; **104**:47–68.
26. Chenais D, Zuazua E. Controllability of an elliptic equation and its finite difference approximation by the shape of the domain. *Numerische Mathematik* 2003; **95**:63–99.
27. Eppler K, Harbrecht H. Second order shape optimization using wavelet BEM. *Optimization Methods and Software* 2006; **21**:135–153.
28. Dennis JE, Schnabel RB. *Numerical Methods for Nonlinear Equations and Unconstrained Optimization Techniques*. Prentice-Hall: Englewood Cliffs, NJ, 1983.
29. Grossmann Ch, Terno J. *Numerik der Optimierung*. Teubner: Stuttgart, 1993.
30. Eppler K, Harbrecht H, Mommer MS. A new fictitious domain method in shape optimization. *Computational Optimization and Applications* 2006; DOI: 10.1007/s10589-007-9076-2. WIAS-Preprint 1117, WIAS Berlin.
31. Greengard L, Rokhlin V. A fast algorithm for particle simulation. *Journal of Computational Physics* 1987; **73**:325–348.
32. Hackbusch W, Khoromskij BN. A sparse $\mathscr{H}$-matrix arithmetic. II: application to multi-dimensional problems. *Computing* 2000; **64**:21–47.
33. Dahmen W, Harbrecht H, Schneider R. Compression techniques for boundary integral equations—optimal complexity estimates. *SIAM Journal on Numerical Analysis* 2006; **43**:2251–2271.
34. Jung M, Steinbach O. A finite element-boundary element algorithm for inhomogeneous boundary value problems. *Computing* 2002; **68**:1–17.
35. Costabel M, Stephan EP. Coupling of finite element and boundary element methods for an elasto-plastic interface problem. *SIAM Journal on Numerical Analysis* 1988; **27**:1212–1226.
36. Han H. A new class of variational formulation for the coupling of finite and boundary element methods. *Journal of Computational Mathematics* 1990; **8**(3):223–232.
37. Harbrecht H, Paiva F, Pérez C, Schneider R. Biorthogonal wavelet approximation for the coupling of FEM–BEM. *Numerische Mathematik* 2002; **92**:325–356.
38. Harbrecht H, Paiva F, Pérez C, Schneider R. Wavelet preconditioning for the coupling of FEM–BEM. *Numerical Linear Algebra with Applications* 2003; **3**:197–222.
39. Kunisch K, Peichl G. Shape optimization for mixed boundary value problems on an embedding domain method. *Dynamics of Continuous*, *Discrete and Impulsive Systems* 1998; **4**:439–478.
40. Neitaanmäki P, Tiba D. An embedding of domain approach in free boundary problems and optimal design. *SIAM Journal on Control and Optimization* 1995; **33**:1587–1602.
41. Slawig T. A formula for the derivative with respect to domain variations in Navier–Stokes flow based on an embedding domain method. *SIAM Journal on Control and Optimization* 2003; **42**:495–512.
42. Glowinski R, Pan TW, Periaux J. A fictitious domain method for Dirichlet problem and applications. *Computer Methods in Applied Mechanics and Engineering* 1994; **111**:283–303.
43. Mommer MS. Towards a fictitious domain method with optimally smooth solutions. *Ph.D. Thesis*, RWTH-Aachen, published online by the RWTH-Aachen, 2005.

44. Mommer MS. A smoothness preserving fictitious domain method for elliptic boundary value problems. *IMA Journal of Numerical Analysis* 2006; **26**:503–524.
45. Braess D. *Finite Elements. Theory*, *Fast Solvers*, *and Applications in Solid Mechanics* (2nd edn). Cambridge University Press: Cambridge, 2001.
46. Bramble JH. *Multigrid Methods*. Pitman Research Notes in Mathematics Series, vol. 294. Longman Scientific & Technical: Harlow, 1993.
47. Hackbusch W. *Multigrid Methods and Applications*. Springer Series in Computational Mathematics, vol. 4. Springer: Berlin, 1985.

DOI: 10.1002/mma